Biosensors and Bioelectronics 142 (2019) 111564

Contents lists available at ScienceDirect

Biosensors and Bioelectronics

journal homepage: www.elsevier.com/locate/bios

Target-induced formation of multiple DNAzymes in solid-state nanochannels: Toward innovative photoelectrochemical probing of telomerase activity

Gao-Chao Fan[a,b], Yanwei Lu[a], Linzheng Ma[a,c], Zhi-Ling Song[a], Xiliang Luo[a,**], Wei-Wei Zhao[b,*]

[a] Key Laboratory of Optic-electric Sensing and Analytical Chemistry for Life Science, MOE, College of Chemistry and Molecular Engineering, Qingdao University of Science and Technology, Qingdao, 266042, China

[b] State Key Laboratory of Analytical Chemistry for Life Science, School of Chemistry and Chemical Engineering, Nanjing University, Nanjing, 210023, China

[c] College of Chemical and Environmental Engineering, Shandong University of Science and Technology, Qingdao, 266590, China

ARTICLE INFO

Keywords:
Photoelectrochemistry
Bioanalysis
Nanochannels
Telomerase activity
DNAzyme

ABSTRACT

Solid-state nanochannels have great potentials in the vibrant field of photoelectrochemical (PEC) bioanalysis. This work herein demonstrates the innovative use of DNA-decorated nanoporous anodic alumina (NAA) nanochannels for sensitive PEC bioanalysis of telomerase (TE) activity. Specifically, telomerase primer sequences (TS) were initially immobilized within the NAA nanochannels and then extended by TE in the presence of deoxyribonucleoside triphosphates (dNTPs). The as formed single-strand DNA was then directed to hybrid with many partially matched single-strand assisting DNA (aDNA), leading to the formation of multiple DNAzymes by the unmatched parts and the subsequent DNAzyme-stimulated biocatalytic precipitation (BCP) within the nanochannels. Because the inhibited signals of the photoelectrode could be correlated with TE-enabled TS extension, an innovative nanochannels PEC bioanalysis could be realized for probing TE activity. This work features the ingenious use of DNA-associated nanochannels for PEC bioanalysis of TE activity. Given the versatile functions of DNA molecules, the extension of this strategy easily allows for addressing numerous other targets of interest. Also, we envision this work could inspire more interest for the further development of nanochannels PEC bioanalysis.

Introduction

In recent years, inspired by the protein nanopores, solid-state nanochannels for smart control of the ionic and molecular transportation have been extensively studied for their great potential in advanced molecular sieves, nanofluidics, energy conversion, and bioanalysis [Ma et al., 2019; Gao et al., 2018; Zhang et al., 2016; Xiao et al., 2016; Sato et al., 2016]. Among the diversified solid-state nanochannels, nanoporous anodic alumina (NAA) membrane is very popular and has been served as a versatile matrix to construct various bioanalysis platforms owning to its characteristics of stability, durability, well-ordered nanochannels, narrow pore-size distribution and especially high surface-to-volume ratio for increased immobilization of guests [Qiao et al., 2019; Ding et al., 2019; Rajeev et al., 2018; Wang et al., 2018]. In addition, the preparation of NAA is easy, controllable, cost-effective, reproducible, and easily up-scalable by mature production techniques.

Photoelectrochemical (PEC) bioassay is a new generation of classic electrochemical method, the detection principle of which is operated upon the produced photocurrent change of the biosystem originating from recognition events between the bioprobes and their target analytes [Zhao et al., 2015]. PEC bioassay has inherited the salient features of simple device, easy-operated instrument, inexpensive sample preparation, and fast signal response from classic electrochemical bioanalysis [Fan et al., 2014]. Moreover, it also owns its unique characteristics: (i) lower background signal and higher sensitivity because of the different energy forms of input and output signals [Zhang et al., 2018a]; (ii) capability for self-powered bioanalysis owning to no use of applied potential [Fan et al., 2019]. Thus, PEC bioassay has roused a great enthusiasm among the analysts. To pursue efficient analysis results, various functional nanomaterials as well as nanostructures with novel signalling mechanisms were explored to address diverse target objects of interest and tremendous advance were achieved. However, given the merits of solid-state nanochannels above, the PEC research in this direction is in its infancy, and very few exploitations have been reported

* Corresponding author.
** Corresponding author.
E-mail addresses: xiliangluo@qust.edu.cn (X. Luo), zww@nju.edu.cn (W.-W. Zhao).

https://doi.org/10.1016/j.bios.2019.111564
Received 2 July 2019; Received in revised form 31 July 2019; Accepted 1 August 2019
Available online 02 August 2019
0956-5663/

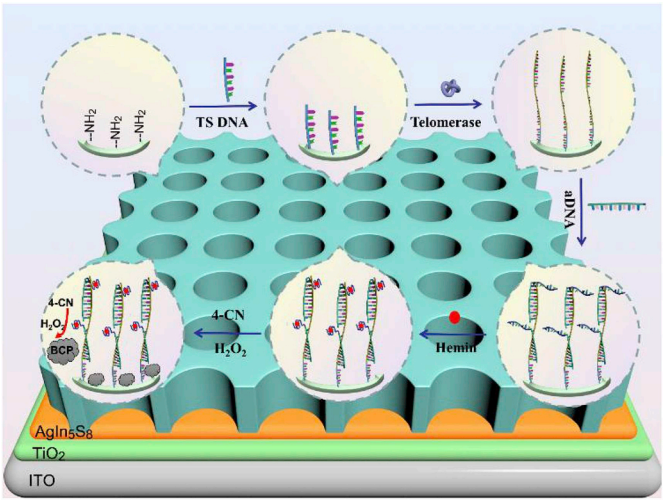

Scheme 1. Schematic illustration for the nanochannels PEC probing of TE activity with HRP-mimicking DNAzyme catalyzed BCP format.

to date [Zhang et al., 2018b]. In this sense, advanced nanochannels PEC bioanalysis that is capable of sensitive bioassay is beyond a doubt highly appealing.

Herein, with the aid of an $AgIn_5S_8/TiO_2$ photoelectrode, this work presents the innovative use of DNA-decorated NAA nanochannels for sensitive PEC bioanalysis of telomerase (TE) activity. Telomerase is a ribonucleoprotein that can maintain telomere length by adding repeated sequences $(TTAGGG)_n$ to the 3' end of telomere, the activity of which is an important parameter for early diagnosis, prognosis and pathogenesis of cancers [Zhou and Xing, 2012; Falchetti et al., 2004; Hahn et al., 1999]. As shown in Scheme 1, the NAA membrane was initially silanized and then immobilized with telomerase primer sequence (TS), which was followed by the extension of TS by TE in the presence of deoxyribonucleoside triphosphates (dNTPs) [Lei et al., 2018; Ling et al., 2016; Liu et al., 2016; Xu et al., 2018]. Further hybridization between the extended DNA with many assisting DNA (aDNA) will generate multiple horseradish peroxidase (HRP)-mimicking G-quadruplexes/hemin DNAzyme [Chu et al., 2019; Ge et al., 2016; Li et al., 2017; Wang et al., 2015], which could catalyze the oxidation between H_2O_2 and 4-chloro-1-naphthol (4-CN) to generate insoluble biocatalytic precipitation (BCP) [Li et al., 2018b; Qileng et al., 2018; Wang et al., 2019; Yang et al., 2018; Zhuang et al., 2015], blocking the nanochannels and inhibiting the photocurrent signal of the photoelectrode. In such a protocol, because the inhibited signals could be correlated with the TE-enabled TS extension, an innovative nanochannels PEC bioanalysis could be realized for probing the TE activity. To our knowledge, such a nanochannels PEC bioanalysis has not been reported for probing TE activity.

2. Experimental

2.1. Materials and reagents

ITO electrodes (sheet resistance ≤ 10 Ω/square, ITO coating 30 ± 5 nm) were ordered from Beijing Zhongjingkeyi Technology Co., Ltd. (China). NAA membranes (60 μm thick, 90 nm aperture) was purchased from Topmembranes Technology Co., Ltd. (China). Triethanolamine, thioacetamide, ammonium nitrate, and silver nitrate were purchased from Alfa Aesar (China). TiO_2 powder (P25), N-hydroxysuccinimide (NHS), indium (III) nitrate hydrate, 1-ethyl-3-(3-(dimethylamino)propyl) carbodiimide hydrochloride (EDC), phenylmethanesulfonyl fluoride (PMSF), (3-aminopropyl)triethoxysilane (APTES), and 3-[(3-cholamidopropyl) dimethyl lammonio]-1-propanesulfonic acid (CHAPS) were obtained from Sigma-Aldrich Inc. (USA). The deoxynucleotide solution mixture (dNTPs), ethylene glycol bis (aminoethyl ether)-N,N,N′,N'-tetraacetic acid (EGTA), and Tween 20 were purchased from Sangon Inc. (Shanghai, China). All other reagents were of analytical grade. All aqueous solutions were prepared with deionized water (DI water, 18 MΩ/cm), obtaining from a Milli-Q water purification system. The telomerase ELISA kit containing a bottle of telomerase standard solution (120 IU/L) was purchased from Jiangsu Ze Yu Biotechnology Co., Ltd. (Yancheng, China). HeLa cell (human cervix adenocarcinoma), HepG2 (human liver cancer cells), and MCF-7 (human breast cancer cells) were obtained from Procell Life Science & Technology Co., Ltd. (Wuhan, China).

All DNA oligonucleotides were synthesized by Sangon Inc. (Shanghai, China) with the sequences as follows:

TS DNA: 5′–COOH–AAA AAA AAT CCG TCG AGC AGA GTT-3'.

aDNA: 5′-CCC TAA CCC TAA CCC TAA TGG GTT GGG CGG GAT GGG-3'.

ACX: 5′-GCG CGG CTT ACC CTT ACC CTT ACC CTA ACC-3'.

In the TS DNA, the underlined sequence was the telomerase primer. In the aDNA, the underlined sequence can form the DNAzyme with G-quadruplexes/hemin format [Yu et al., 2014; Zhou and Xing, 2012]. The TS DNA and aDNA were used for nanochannels PEC bioanalysis, while the TS DNA and ACX were used for telomeric repeat amplification protocol (TRAP) assay as the control experiment.

2.2. Apparatus

Field-emission scanning electron microscopy (FE-SEM) was carried out on a Hitachi S-4800 scanning electron microscope (Hitachi Co., Japan). Powder X-ray diffraction (XRD) pattern was obtained from a Philips X'pert Pro X-ray diffractometer (Cu Kα radiation, λ = 0.15418 nm, Netherlands). X-ray photoelectron spectroscopy (XPS) was performed using an ESCALAB 250Xi spectrometer (Thermo Fisher Scientific, UK) with a monochromatic Al Kα X-ray source, and all spectra were calibrated by normalizing the C (1s) peak to the standard value of 284.6 eV. Photoluminescence (PL) spectra were recorded by an F-7000 fluorescence spectrometer (Hitach, Japan). Electrochemical impedance spectroscopy (EIS) was performed on an Autolab potentiostat/galvanostat (PGSTAT 30, Eco Chemie B.V., Utrecht, Netherlands) with a three-electrode system in 0.1M KCl solution containing 5.0 mM K_3 $[Fe(CN)_6]/K_4$ $[Fe(CN)_6]$ (1:1) mixture as a redox probe, and recorded in the frequency range of 0.01 Hz–100 kHz with an amplitude of 50 mV. PEC tests were performed with Zahner PEC workstation (ZAHNER-elektrik GmbH & Co. KG, Germany) with a conventional three-electrode system: a platinum wire as counter electrode, a saturated Ag/AgCl electrode as reference electrode and a modified $AgS_{5I}n_8/TiO_2$/ITO photoelectrode with an area of 0.5 × 0.5 cm^2 as working electrode.

2.3. Cell culture and telomerase extraction

HeLa, HepG2, and MCF cells were grown in Dulbecco's minimal essential (DMEM) medium (Gibco, Grand Island, NY) supplemented with 10% fetal bovine serum (FBS) (Gibco, Grand Island, NY), penicillin (100 μg/mL), and streptomycin (100 μg/mL) in incubator at 37 °C under 5% CO_2 atmosphere. Cell number was determined using a blood counting chamber.

About 1.0×10^6 cells in 1 mL of cell culture medium were transferred into a 1.5 mL EP tube and washed twice with ice cold phosphate buffer solution (PBS, pH 7.4, 0.1 M) by centrifugation at 2000 rpm for 5 min at 4 °C. The cells were resuspended in 200 μL of ice-cold CHAPS lysis buffer (10 mM Tris-HCl, pH 7.5, 1 mM $MgCl_2$, 1 mM EGTA, 0.5% (w/v) CHAPS, 10% (v/v) glycerol, 0.1 mM PMSF) and kept for 30 min in an ice bath. The lysate was centrifuged at 12 000 rpm for 20 min at 4 °C. The resulting extract was carefully frozen at −80 °C or used immediately. For the control experiment, the telomerase extract was heat-treated at 95 °C for 10 min prior to detection.

2.4. Conventional TRAP assay

The telomeric repeat amplification protocol (TRAP) assay was conducted as follows. 5 mL of telomerization products were added into 45 μL of solution, which contains 1 × polymerase chain reaction (PCR) buffer, 200 mM dNTPs, 2.5 U of Taq DNA polymerase, 0.4 mM TS primer and 0.4 mM ACX primer. PCR was carried out using T100 (Bio-Rad, USA) thermal cycler with the following program: 94 °C for 5 min; 30 cycles at 94 °C for 30 s, 59 °C for 30 s, and 72 °C for 30 s; 72 °C for 5 min; 4 °C hold. PCR products were analyzed using a vertical electrophoresis system. The native polyacrylamide gel electrophoresis (PAGE) was performed in a vertical gel system. Gel stock solution (30%, w/v) contained 7.3 g acrylamide and 0.2 g bis(N,N′-methylenebisacrylamide), which were dissolved in 25 mL of H_2O and filtrated. Gels were prepared by mixing 4.0 mL of gel stock solution, 8.0 mL of ultrapure water, 4 mL of Tris-HCl (1.5 M, pH 8.8), 150 μL of $(NH4)_2S_2O_8$ (10%, w/v) and 15 μL of TEMED. The voltage was set at 135 V for about 0.5 h. Then, the gel slabs were stained in the Gel Red solution in the dark for 1 h. At last, the fluorescence image was recorded by a bioimaging system (UVP EC3 Imaging System, UVP, Inc., USA) at the wavelength of 365 nm. (The loading volume for each channel was 10 μL)

2.5. Preparation of $AgIn_5S_8/TiO_2$/ITO photoelectrode

Before preparation, ITO slices were cleaned by ultrasonic treatment for 10 min in acetone, 1 M NaOH of water/ethanol mixture (1:1, v/v), and water, respectively, and then dried at 100 °C for 6 h. A certain amount of TiO_2 powder was ultrasonically dispersed in DI water, and then 20 μL of the homogeneous suspension was applied onto a piece of ITO slice with fixed area of 0.25 cm^2. After drying in air, the film was sintered at 450 °C for 30 min in air atmosphere and cooled down to room temperature, and termed as TiO_2/ITO electrode. In order to acquire different thicknesses of TiO_2 film, the concentrations of TiO_2 suspension were varied to 0.5, 0.75, 1.0, 1.25, 1.5 and 2.0 mg/mL.

The $AgIn_5S_8/TiO_2$/ITO photoelectrode was fabricated according to a previous report with some modifications [Guan et al., 2018a,b]. Silver nitrate ($AgNO_3$), indium nitrate ($In(NO_3)_3$), and thioacetamide (CH_3CSNH_2, TAA) were the sources of Ag^+, In^{3+}, and S^{2-} ions, respectively. Triethanoamine ($C_6H_{15}NO_3$, TEA) and ammonium nitrate (NH_4NO_3) were chelating agent and buffer, respectively. The solution consisted of 1.09 mL of 0.3 M $AgNO_3$, 1.09 mL of 0.3 M $In(NO_3)_3$, 0.55 mL of 0.3 M NH_4NO_3, and 0.55 mL of 7.4 M TEA. Sulfuric acid was used to adjust the pH value of the cationic solution to 1.2 in order to avoid the formation of hydroxide complexes such as $In(OH)_3$. The solution was stirred for 0.5 h, and then 15.3 mL of 0.3 M TAA solution was added. The TiO_2/ITO electrode was placed vertically into the reaction bath. The temperature of the reaction bath was kept at 80 °C, and the reaction time was set for 1.5 h. The deposited samples were washed with DI water to remove loosely bound particles on the film. The $AgIn_5S_8/TiO_2$/ITO electrode with different loading amounts of $AgIn_5S_8$ were prepared by changing the amount of $AgNO_3$ and $In(NO_3)_3$ under the same method.

2.6. Modification of NAA with TS primer

The modification of NAA nanochannels with TS primer was achieved in two main steps: (i) generation of amino groups on the nanochannels by a silanization with APTES [Liu et al., 2018; Yu et al., 2014]; (ii) immobilization of carboxyl-modified TS primer by the classic EDC coupling reaction [Zhang et al., 2018b]. First, NAA membrane was washed with ethanol and ultrapure water to remove the impurities in nanochannels. After being dried under N_2, the NAA membrane was immersed in 1 mL of an ethanol solution containing 5% APTES and kept at 4 °C overnight to generate amino groups on the surface and inside the channels. By shaking the NAA membrane gently in ethanol several times (10 min each), excess APTES was washed out. Then the NAA membrane was immersed into 1 mL of 5 mM EDC-NHS containing 1.5 μM TS primer, left to incubate for 16 h at 4 °C, and then washed with PBS (pH 7.4, 0.1 M) several times to remove the physically absorbed TS primer.

2.7. Construction of nanochannels PEC bioanalysis

For telomerase extension reaction, 20 μL of telomerase reaction solution containing 10 μL of telomerase extracts which contained specified number of HeLa cells or standard telomerase, and 2 mM dNTPs in 1 × TRAP buffer (20 mM Tris-HCl pH 8.3, 1.5 mM $MgCl_2$, 63 mM KCl, 0.005% Tween 20, 1 mM EGTA) were pipetted onto the surface of the TS-modified NAA membrane and incubated at 37 °C for 2 h. Heat-deactivated control experiment was implemented by heat-treated telomerase extracts (95 °C for 10 min). Then the NAA membrane modified with extended-TS was immersed in the solution containing 1 μM aDNA at 4 °C for 3 h. After thoroughly washed with PBS (0.1 M, pH 7.4) to remove the unbound aDNA, the modified NAA membrane was immerged into 0.5 mL of the reaction solution containing 5 mM KCl and 1 μM hemin, followed by keeping at room temperature for 60 min to form the G-quadruplexes/hemin DNAzyme. After again rinsed with PBS (0.1 M, pH 7.4), the G-quadruplexes-loaded membrane was immersed into 0.5 mL of 1.0 mM 4-CN containing 0.15 mM H_2O_2 and incubated for 15 min to induce the enzymatic biocatalytic precipitation reaction. After washed with DI water, the NAA membrane was compactly fixed onto the conducting side of the $AgIn_5S_8/TiO_2$/ITO photoelectrode by physical attachment of a black gummed tape with a 1 mm × 5 mm working area. Finally, a PEC measurement was conducted with the light irradiating from the back.

2.8. PEC measurement

The PEC detection was carried out at room temperature in PBS (pH 7.4, 0.1 M) containing 0.1 M ascorbic acid (AA), which acted as sacrificial reagents providing electrons to the photoelectrode. A LED lamp with a spectral 430 nm was utilized as irradiation source with light intensity of 350 W/m^2, which was switched on and off every 10 s. The applied electrochemical method was chopped light voltammetry, and the applied voltage was 0.0 V.

3. Results and discussion

3.1. Characterization of $AgIn_5S_8/TiO_2$/ITO photoelectrode

The surface morphology of the $AgIn_5S_8/TiO_2$/ITO photoelectrode for its fabrication process was first monitored by SEM, as shown in Fig. 1a and b. When TiO_2 film was covered on the surface of the ITO electrode (Fig. 1a), plenty of TiO_2 nanoparticles with grain size of 22–28 nm were observed, and the formed mesoporous film had large specific surface area for subsequent photoactive material modification. After $AgIn_5S_8$ further deposition (Fig. 1b), the surface was full covered with the layer structures with abundant wrinkles. The elemental mapping analysis in the insets of Fig. 1a and b also reflected the deposition of $AgIn_5S_8$ on the TiO_2/ITO electrode.

The XRD patterns of the TiO_2 and $AgIn_5S_8/TiO_2$ nanocomposite are shown in Fig. 1c. For the TiO_2 layer (black curve), the diffraction peaks showed (101) and (200) plane of the anatase TiO_2 and (110) plane of the rutile TiO_2. After modification of $AgIn_5S_8$ layer (red curve), the newly appeared diffraction peaks at 2θ = 15.2°, 23.1°, 26.8°, 28.5°, 32.8°, 41.2°, 42.9°, and 47.7° can be attributed to the (111), (220), (311), (222), (400), (422), (511), and (440) planes of pure cubic $AgIn_5S_8$ (JCPDS NO. 26–1477), respectively, which indicated successful formation of the $AgIn_5S_8/TiO_2$ nanocomposite. XPS was also utilized to determine chemical composition and valence states of the $AgIn_5S_8/TiO_2$ nanocomposite, as shown in Fig. 1d. The spectrum shows XPS peaks of Ti 3p, S 2p, S 2s, C 1s, Ag 3d, In 3d, Ti 2p, O 1s, and In 3d peaks. Among these XPS peaks, Ti 3p, Ti 2p and O 1s was from TiO_2, and S 2p, S 2s, Ag 3d, In 3d and In 3d were from $AgIn_5S_8$. XPS peak for C 1s was used as

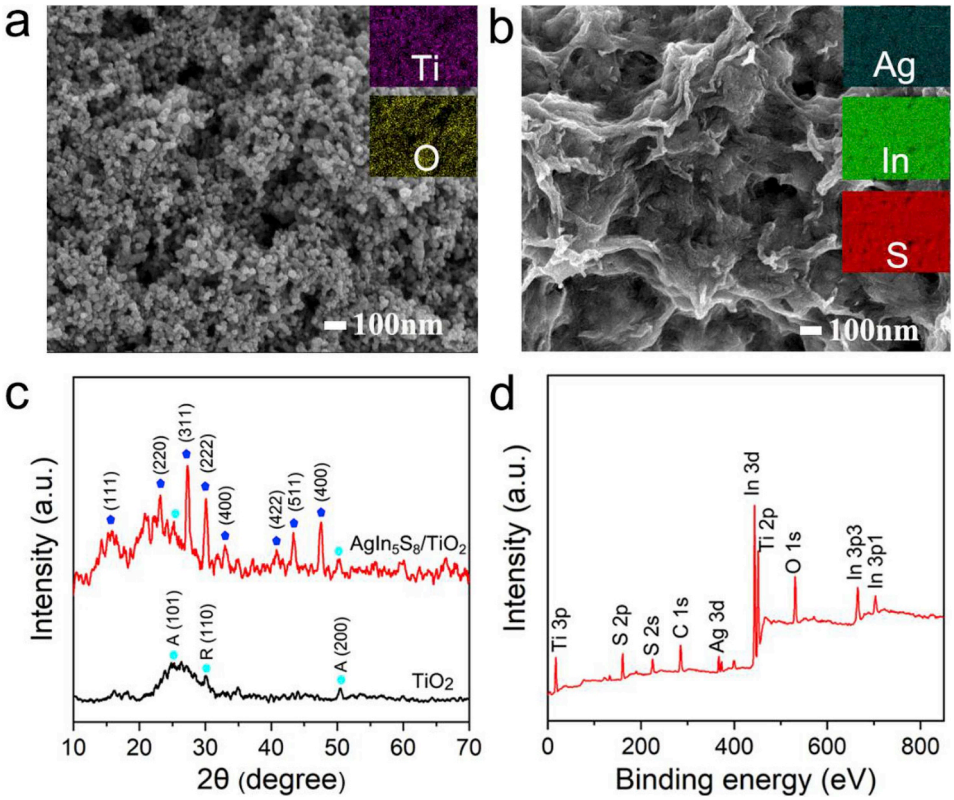

Fig. 1. SEM images of (a) the TiO_2/ITO and (b) the $AgIn_5S_8/TiO_2$/ITO electrode; (c) XRD patterns of the TiO_2 and $AgIn_5S_8/TiO_2$ nanocomposite; (d) XPS spectrum of the $AgIn_5S_8/TiO_2$ nanocomposite. Insets in panels a and b: elemental mapping analysis of (Ti and O) and (Ag, In, and S), respectively.

the internal reference to correct the binding energy. Thus, XPS characterization further proved the successful fabrication of the $AgIn_5S_8/TiO_2$/ITO photoelectrode.

3.2. PEC behavior of $AgIn_5S_8/TiO_2$/ITO photoelectrode

Fig. 2a shows photocurrent response of the $AgIn_5S_8/TiO_2$/ITO photoelectrode for its stepwise fabrication. The TiO_2 modified ITO electrode showed a relatively low photocurrent response (curve a). After $AgIn_5S_8$ was then modified (curve b), the photocurrent response evidently increased, which was nearly 5 times higher than that of the TiO_2/ITO electrode. On the basis of the photocurrent responses above and band positions of TiO_2 and $AgIn_5S_8$, the PEC process of the $AgIn_5S_8/TiO_2$/ITO electrode was illustrated in Fig. 2b. TiO_2 is an n-type semiconductor with high photoelectric activity, stability, biocompatibility and low cost, making it very suitable for serving as the PEC matrix [Fan et al., 2016]. Yet, TiO_2 has a wide-band gap (~3.2 eV), which can only absorb the ultraviolet light, resulting in a relatively low photocurrent response. As a kind of ternary sulfide compound, $AgIn_5S_8$ is a very promising material for fabricating an efficient photoelectrode because of its excellent balance of strong visible-light responsivity and nontoxicity. $AgIn_5S_8$ has a direct bandgap (1.70–1.80 eV), which could allow the photons in the UV–vis range (< 700 nm) to excite [Guan et al., 2018a,b; Kan et al., 2013]. Besides, the conduction band (CB) and valence band (VB) edges of $AgIn_5S_8$ are both higher than that of TiO_2, resulting in the fast injection of excited electrons from $AgIn_5S_8$ to TiO_2 [Guan et al., 2018a,b; Kan et al., 2013]. Therefore, the $AgIn_5S_8/TiO_2$ hybrid can significantly expand the spectral absorption range and dramatically inhibit the electron-hole recombination, and thereby enhance the photocurrent response evidently.

The photogenerated carrier separation efficiency in the $AgIn_5S_8/TiO_2$ hybrid was confirmed by the photoluminescence (PL) spectra, as shown in Fig. 2c. It was found that the fluorescence signal of the $AgIn_5S_8/TiO_2$ hybrid was evidently reduced compared to signal TiO_2, indicating that the photogenerated carrier recombination was inhibited greatly [Guan et al., 2018a,b; Li et al., 2015; Li et al., 2013]. The result stemmed from the interface contact between TiO_2 and $AgIn_5S_8$. In order to test the stability of the $AgIn_5S_8/TiO_2$/ITO photoelectrode, time-varying photocurrent intensity was performed, as displayed in Fig. 2d. It can be observed that the photocurrent intensity remained almost unchanged under each irradiation period, and there was no significant attenuation when the photoelectrode encountered repeated light illumination, indicating the $AgIn_5S_8/TiO_2$/ITO photoelectrode was highly stable.

3.3. SEM observation of nanochannels-based BCP reaction

The unique properties of NAA membrane have made it an excellent platform with great opportunities for development of advanced, smart, simple, cost-effective sensing and biosensing devices for specific analytical applications [Guo et al., 2015; Long et al., 2018; Zhang et al., 2018b]. To reveal the feasibility of the proposed nanochannels system in this work, SEM observation was conducted to disclose morphological information associated with the NAA nanochannels that corresponded to varying TE activity. As demonstrated in Fig. 3a, the pristine NAA membrane exhibits as close-packed perpendicular arrays of hexagonally-arranged cells containing cylindrical central pores with an average diameter of ca. 100 nm. The cross-sectional view reveals the hollow nanochannels with smooth inner surface. Obviously, such a nanostructure with much enhanced surface-to-volume ratio would be advantageous to biomolecular immobilization, recognition reaction, and signal enhancement. After TE extension reaction and BCP stimulation corresponding to 5000 and 5.0×10^5 HeLa cells/mL, as shown in Fig. 3b and c, a lot of BCP was generated onto the NAA surface and into the nanochannels. As shown in Fig. 3d–f, with the enhanced TE activity, the BCP was getting thicker with more narrowed internal apertures. The above SEM observation validated the successful formation of multiple DNAzymes and the resultant BCP within the nanochannels.

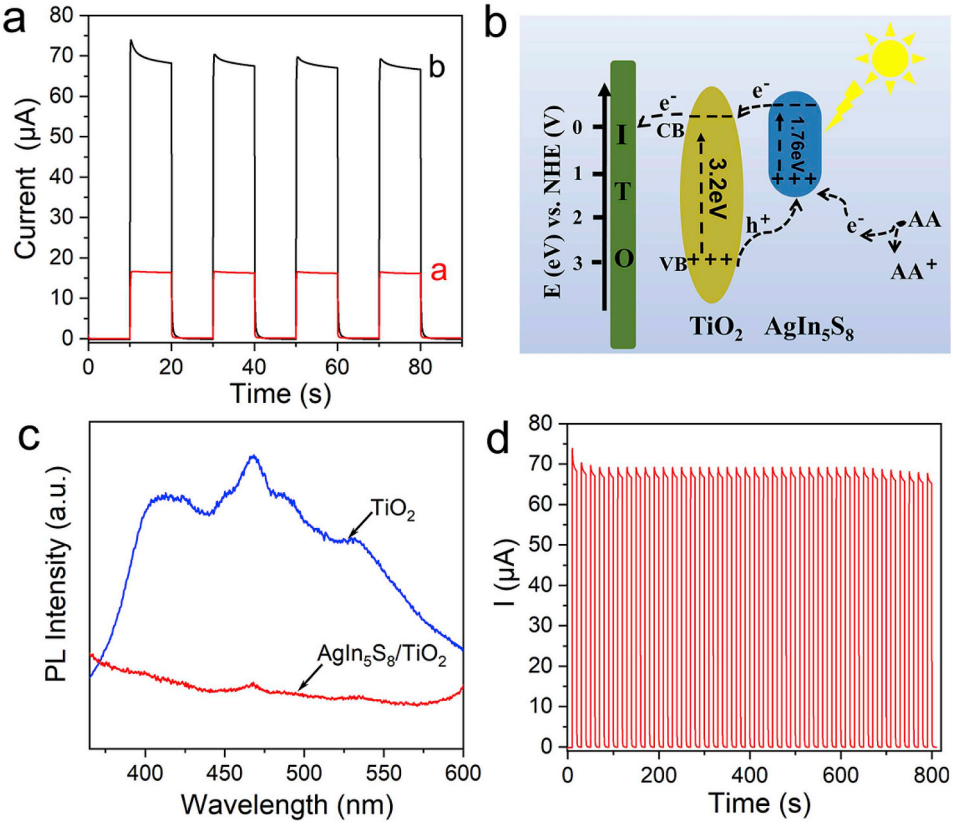

Fig. 2. (a) Photocurrent response of the TiO_2/ITO (curve a) and $AgIn_5S_8/TiO_2$/ITO (curve b) electrodes; (b) schematic illustration for the PEC process of the $AgIn_5S_8/TiO_2$/ITO electrode; (c) PL spectra of the TiO_2 and $AgIn_5S_8/TiO_2$ nanocomposite; (d) time-varying photocurrent response of the $AgIn_5S_8/TiO_2$/ITO photoelectrode.

3.4. Characterization of nanochannels PEC bioanalysis

Based on PEC matrix of the $AgIn_5S_8/TiO_2$/ITO photoelectrode, the development of the nanochannels PEC bioanalysis was first characterized by photocurrent responses, as shown in Fig. 4a. The $AgIn_5S_8/TiO_2$/ITO photoelectrode exhibited an evident photocurrent response (curve a). After NAA membrane anchoring, a visible decrease in photocurrent was observed due to the large steric resistance (curve b). After TS DNA modification, TE extension reaction and aDNA hybridization in sequence, slightly reduction of the photocurrent response in each step occurred (curves c-e), due to relatively weak charge transfer of DNA molecules [Hao et al., 2018; Li et al., 2018a; Zeng et al., 2019]. After the hemin modified electrode was incubated with 4-CN coexisting with H_2O_2, the photocurrent response weakened dramatically (curve f). It was because the nanochannels of the NAA membrane were gradually blocked by the induced enzymatic biocatalytic precipitation, and thereby, the reduced aperture of the

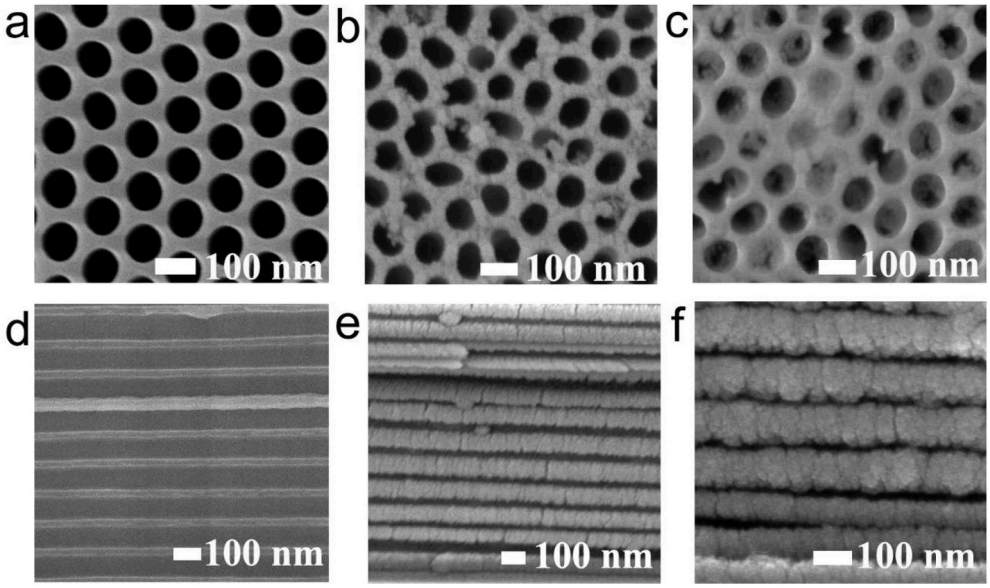

Fig. 3. (a–c) Top and (d–f) cross-sectional view of SEM images of the NAA membrane before and after the BCP reaction corresponding to (a, d) 0, (b, e) 5000, and (c, f) 5×10^5 cells/mL of HeLa cells.

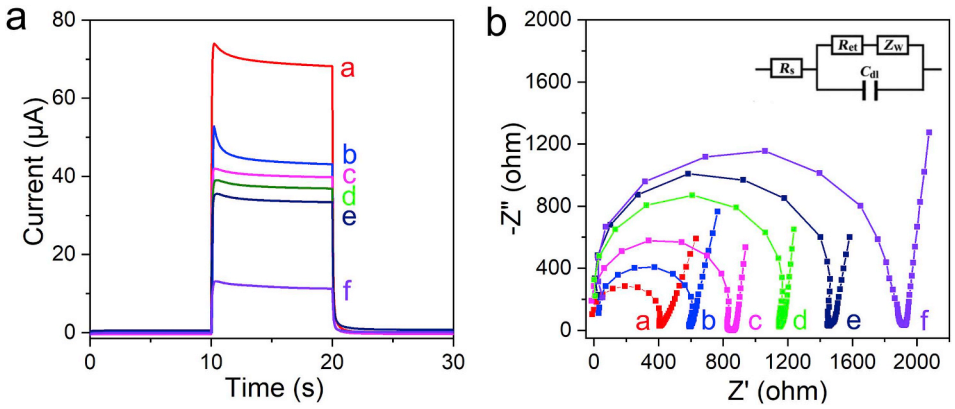

Fig. 4. (a) Photocurrent responses and (b) EIS of the $AgIn_5S_8/TiO_2$/ITO photoelectrode (curve a), after blank NAA membrane anchoring (curve b), after TS DNA modification (curve c), after TE extension reaction (curve d), after incubation with aDNA (curve e), and after incubation with 1.0 mM 4-CN containing 0.15 mM H_2O_2 for 15 min (curve f). Inset of (b): the electrical equivalent circuit fitted the impedance spectra; R_{et}, Z_w, C_{dl}, and R_s stand for electron transfer resistance, Warburg impedance, double-layer capacitance, and ohmic resistance of the electrolyte, respectively.

nanochannels would make the light source energy and the electron donor of AA more difficult to access the PEC matrix of the $AgIn_5S_8/TiO_2$/ITO photoelectrode via the nanochannels.

As an effective method to study the interface properties, electrochemical impedance spectroscopy (EIS) of the nanochannels PEC bioanalysis was also performed, as displayed in Fig. 4b. The semicircle diameters of the curves reflect the electron-transfer resistance (R_{et}). For the $AgIn_5S_8/TiO_2$/ITO photoelectrode, a relatively small R_{et} was observed (curve a). After blank NAA membrane anchoring, the R_{et} increased moderately because of its low conductivity (curve b). After stepwise procedures of TS DNA modification, TE extension reaction and aDNA hybridization, the R_{et} elevated step by step (curves c-e), which was all attributed to low conductivity of the DNA molecules. After the hemin modified electrode underwent the incubation of 4-CN containing H_2O_2, the R_{et} increased evidently (curve f), which indicated successful formation of the multiple DNAzymes and the resultant BCP within the NAA nanochannels. The EIS results agreed well with the photocurrent responses of the PEC bioanalysis development. Obviously, the steric hindrance degree associated closely with the TE activity, the higher of which would cause enhanced signal inhibition.

3.5. Performances of nanochannels PEC bioanalysis

In order to evaluate detection performances of the nanochannels PEC bioanalysis, the optimal experimental conditions were first explored (see Fig. S1 and its description) and then HeLa cells as a model was selected for sensitive quantification of TE activity. The photocurrent responses toward HeLa cells with varied concentrations were recorded. As shown in Fig. 5a, with increase in the concentration of HeLa cells, the amount of telomerase was accumulated, causing more amount of BCP to block the NAA channels, and as a result, the photocurrent response displayed a gradual decrease. As exhibited in Fig. 5b,

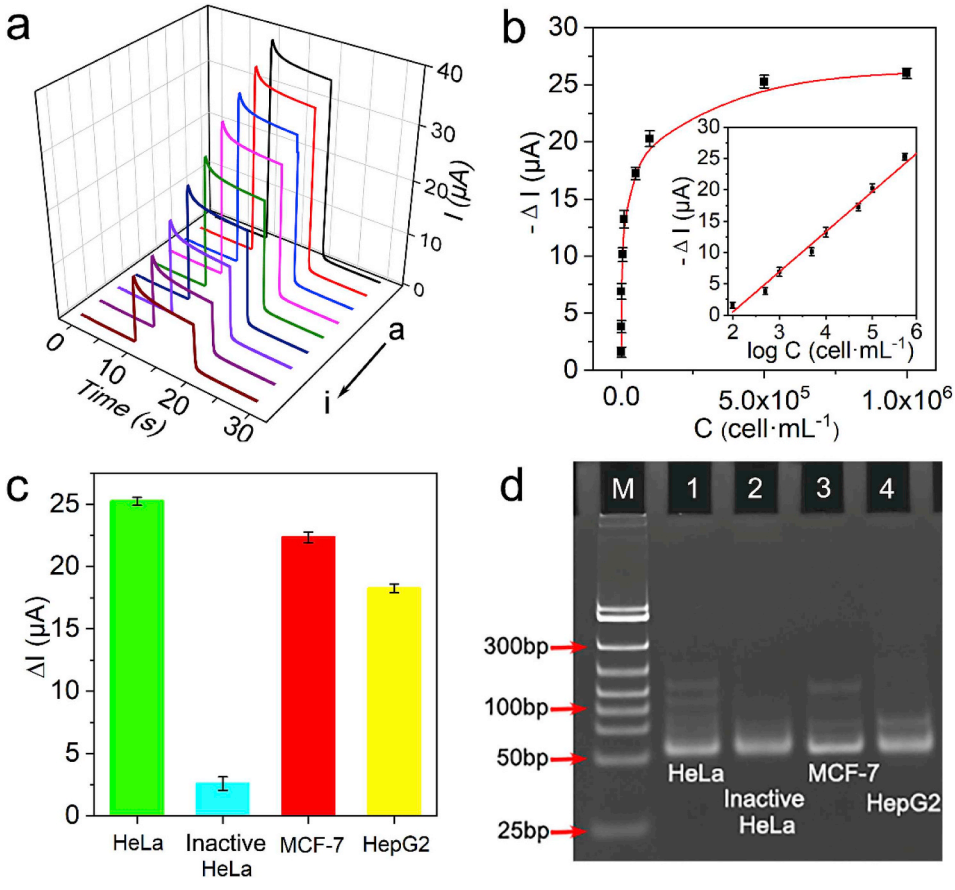

Fig. 5. (a) Photocurrent signals of the nanochannels PEC bioanalysis toward increasing concentrations of HeLa cells (curve a to i). (b) Plot of photocurrent change ($-\Delta I$) versus HeLa cell concentration; Inset of (b), calibration curve between $-\Delta I$ and logarithm of HeLa cell concentration. (c) TE activity of different cell lines tested by nanochannels PEC bioanalysis (the cell number of each was 1.0×10^6). (d) Classical TRAP assay for TE activity. Lines left to right show HeLa, heat-inactive HeLa, MCF-7 and HepG2 cancer cells, respectively. The error bars show standard deviation of five parallel measures.

within the wide range of the concentration from 100 cell/mL to 5×10^5 cells/mL, the photocurrent signal enlarged linearly with an increase of the logarithm of the HeLa cells concentration. The regression equation was $-\triangle I = -12.31 + 6.40 \log C$ (cell/mL), with a correlation coefficient of 0.992. The limit of detection (LOD) was calculated to be 35 cell/mL (S/N = 3), which was lower than or comparable with many previous reports as listed in Table S1.

The general and reliable applicability of the nanochannels PEC bioanalysis for TE activity detection was then assessed by using different cell lines including HeLa, inactive HeLa, MCF-7 and HepG2. The photocurrent signals for TE activity toward different cell lines were revealed, as shown in Fig. 5c. All the active cancer cell lines caused evident photocurrent signals, indicating positive role for telomerase activity. While a very weak photocurrent signal as background for TE activity was observed in the control group with heat-inactive HeLa cell extracts, which was ascribed to the lack of telomerase activity. The control test confirmed favourable selectivity of the nanochannels PEC bioanalysis for TE activity detection.

Furthermore, in order to verify the accuracy of the nanochannels PEC bioanalysis, classical telomeric repeat amplification protocol (TRAP) assay was also employed to measure the corresponding cell extracts above. As displayed in Fig. 5d, except the heat-inactive HeLa cancer cells, all the active cancer cell lines showed evident TE amplification product bands, demonstrating the high TE activity in these cancer cells. The results of the nanochannels PEC bioanalysis was in accordance with the TRAP assay and it could also distinguish the levels of TE activity toward different cell lines.

Conclusion

In summary, this work reported the sensitive PEC bioanalysis of TE activity that operated upon an innovative nanochannels system. In such a system, NAA membrane was used to accommodate the DNA immobilization, extension, recognition and formation of multiple DNAzymes. Because the as-formed DNAzyme could mimic the HRP to stimulate the BCP event within the nanochannels, the inhibited signals of the photoelectrode could thus be correlated with the TE-enabled TS extension. In the probing of TE activity, the as-developed system shows the potential to differentiate various cancer cells and inactive ones, which was confirmed by the classical TRAP assay. In all, this work firstly used the DNA-associated nanochannels for sensitive PEC bioanalysis of TE activity. More generally, given the versatile functions of DNA molecules, this protocol could be easily extended for building of other DNA-based nanochannels PEC bioanalysis toward numerous targets of interest.

CRediT authorship contribution statement

Gao-Chao Fan: Conceptualization, Data curation, Visualization, Writing - original draft. **Yanwei Lu:** Investigation, Methodology. **Linzheng Ma:** Investigation, Methodology. **Zhi-Ling Song:** Formal analysis. **Xiliang Luo:** Supervision, Writing - review & editing. **Wei-Wei Zhao:** Supervision, Writing - review & editing.

Acknowledgments

This work was supported by the National Natural Science Foundation of China (21603099), the Taishan Scholar Program of Shandong Province of China (ts20110829), and the Project Fund for Shangdong Key R&D Program (2019GSF108175).

Appendix A. Supplementary data

Supplementary data to this article can be found online at https://doi.org/10.1016/j.bios.2019.111564.

References

Chu, Y., Deng, A.P., Wang, W., Zhu, J.J., 2019. Anal. Chem. 91, 3619–3627.
Ding, D., Gao, P., Ma, Q., Wang, D., Xia, F., 2019. Small. https://doi.org/10.1002/smll.201804878.
Falchetti, M.L., Pallini, R., Levi, A., 2004. Am. J. Cancer 3, 1–11.
Fan, G.C., Lu, Y., Zhao, H., Liu, Q., Li, Z., Luo, X., 2019. Biosens. Bioelectron. 137, 52–57.
Fan, G.C., Zhu, H., Du, D., Zhang, J., Zhu, J.J., Lin, Y., 2016. Anal. Chem. 88, 3392.
Fan, G.C., Ren, X.L., Zhu, C., Zhang, J.R., Zhu, J.J., 2014. Biosens. Bioelectron. 59, 45–53.
Gao, P., Ma, Q., Ding, D., Wang, D., Lou, X., Zhai, T., Xia, F., 2018. Nat. Common. 9, 4557.
Ge, L., Wang, W., Hou, T., Li, F., 2016. Biosens. Bioelectron. 77, 220–226.
Guan, P., Bai, H., Li, C., Ge, Y., Xu, D., Chen, B., Xia, T., Fan, W., Shi, W., 2018a. Adv. Mater. Interfaces 5, 1701574.
Guan, Z., Xu, Z., Li, Q., Wang, P., Li, G., Yang, J., 2018b. Appl. Catal. B Environ. 227, 512–518.
Guo, W., Hong, F., Liu, N., Huang, J., Wang, B., Duan, R., Lou, X., Xia, F., 2015. Adv. Mater. 27, 2090–2095.
Hahn, S.A., MW, B., SG, Y., E, E., A, K., RL, B., JH, K., M, M., RA, W., 1999. Nat. Med. 5, 1164–1170.
Hao, N., Hua, R., Zhang, K., Lu, J., Wang, K., 2018. Anal. Chem. 90, 13207–13211.
Kan, L., Bo, C., Peng, T., Jing, M., Ling, Z., 2013. ACS Catal. 3, 170–177.
Lei, J., Han, B., Lv, S., Li, Y., Tang, J., Mao, Y., Zhuang, J., 2018. Electrochem. Commun. 92, 43–47.
Li, H., Yu, K., Lei, X., Guo, B., Fu, H., Zhu, Z., 2015. J. Phys. Chem. C 119, 22681–22689.
Li, K., Chai, B., Peng, T., Mao, J., Zan, L., 2013. ACS Catal. 3, 170–177.
Li, L., Zheng, X., Huang, Y., Zhang, L., Cui, K., Zhang, Y., Yu, J., 2018a. Anal. Chem. 90, 13882–13890.
Li, M., Tian, X., Liang, W., Yuan, R., Chai, Y., 2018b. Anal. Chem. 90, 14521–14526.
Li, R., Zhang, Y., Tu, W., Dai, Z., 2017. ACS Appl. Mater. Interfaces 9, 22289–22297.
Ling, P., Lei, J., Ju, H., 2016. Anal. Chem. 88, 10680–10686.
Liu, X., Wei, M., Liu, Y., Lv, B., Wei, W., Zhang, Y., Liu, S., 2016. Anal. Chem. 88, 8107–8114.
Liu, Y., Fan, J., Yang, H., Xu, E., Wei, W., Zhang, Y., Liu, S., 2018. Biosens. Bioelectron. 113, 136–141.
Long, Z., Zhan, S., Gao, P., Wang, Y., Lou, X., Xia, F., 2018. Anal. Chem. 90, 577–588.
Ma, Q., Si, Z., Li, Y., Wang, D., Wu, X., Gao, P., Xia, F., 2019. Trac. Trends Anal. Chem. 115, 174–186.
Qiao, Z., Zhang, H., Zhou, Y., Zheng, J., 2019. Anal. Chem. 91, 5125–5132.
Qileng, A., Wei, J., Lu, N., Liu, W., Cai, Y., Chen, M., Lei, H., Liu, Y., 2018. Biosens. Bioelectron. 106, 219–226.
Rajeev, G., Simon, B.P., Marsal, L.F., Voelcker, N.H., 2018. Adv. Healthc. Mater. 7, 1700904.
Sato, S., Unemoto, A., Ikeda, T., Orimo, S., Isobe, H., 2016. Small 12, 3381–3387.
Wang, G.L., Liu, K.L., Shu, J.X., Gu, T.T., Wu, X.M., Dong, Y.M., Li, Z.J., 2015. Biosens. Bioelectron. 69, 106–112.
Wang, J., Hou, J., Zhang, H., Tian, Y., Jiang, L., 2018. ACS Appl. Mater. Interfaces 10, 2033–2039.
Wang, M., Yin, H., Zhou, Y., Sui, C., Wang, Y., Meng, X., Waterhouse, G.I.N., Ai, S., 2019. Biosens. Bioelectron. 128, 137–143.
Xiao, K., Wen, L., Jiang, L., 2016. Small 12, 2810–2831.
Xu, S., Jiang, L., Nie, Y., Wang, J., Li, H., Liu, Y., Wang, W., Xu, G., Luo, X., 2018. ACS Appl. Mater. Interfaces 10, 26851–26858.
Yang, R., Zou, K., Li, Y., Meng, L., Zhang, X., Chen, J., 2018. Anal. Chem. 90, 9480–9486.
Yu, J., Zhang, L., Xu, X., Liu, S., 2014. Anal. Chem. 86, 10741–10748.
Zeng, R., Luo, Z., Su, L., Zhang, L., Tang, D., Niessner, R., Knopp, D., 2019. Anal. Chem. 91, 2447–2454.
Zhang, H., Tian, Y., Jiang, L., 2016. Nano Today 11, 61–81.
Zhang, K., Lv, S., Lin, Z., Li, M., Tang, D., 2018a. Biosens. Bioelectron. 101, 159–166.
Zhang, N., Ruan, Y.F., Zhang, L. Bin, Zhao, W.W., Xu, J.J., Chen, H.Y., 2018b. Anal. Chem. 90, 2341–2347.
Zhao, W.W., Xu, J.J., Chen, H.Y., 2015. Chem. Soc. Rev. 44, 729–741.
Zhou, X.M., Xing, D., 2012. Chem. Soc. Rev. 41, 4643–4656.
Zhuang, J., Lai, W., Xu, M., Zhou, Q., Tang, D., 2015. ACS Appl. Mater. Interfaces 7, 8330–8338.